

PAPER • OPEN ACCESS

Probing protein surface interactions in nanoaperture optical tweezers

To cite this article: Sherin George et al 2025 Nanotechnology 36 475501

View the article online for updates and enhancements.

You may also like

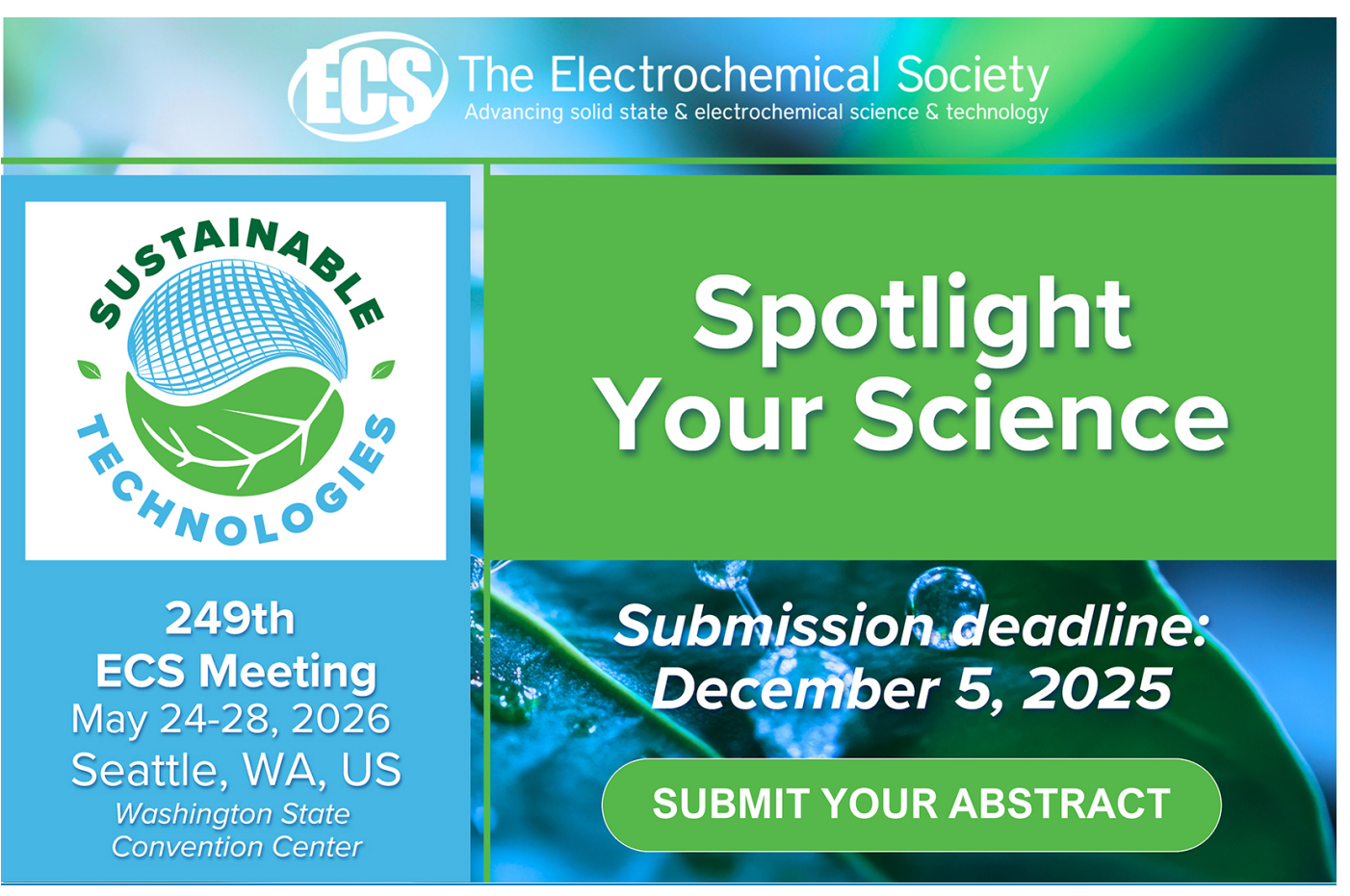
 Ultra-low-energy skyrmion-based learning automata element for adaptive edge intelligence

Kishore C, Santhosh Sivasubramani, Sarwath Sara C et al.

 Ohmic contact engineering for twodimensional material-based field-effect transistors: recent advances and perspectives

perspectives
Zichao Ma, Jiwei Chen, Zhixin Chen et al.

- <u>SnO₂ based nanostructures for gas sensor application: a review</u>
Goda Vasantharao and Jay Chandra Dhar



Nanotechnology 36 (2025) 475501 (8pp)

https://doi.org/10.1088/1361-6528/ae1c48

Probing protein surface interactions in nanoaperture optical tweezers

Sherin George^{1,2,5}, Tianyu Zhao^{1,2,5}, Keiran Letwin^{1,2}, Viet Giang Truong³, Naser Helmi^{1,2}, Síle Nic Chormaic³, Cuifeng Ying⁴ and Reuven Gordon^{1,2,*}

E-mail: rgordon@uvic.ca

Received 15 April 2025, revised 15 October 2025 Accepted for publication 6 November 2025 Published 19 November 2025



Abstract

Nanoaperture optical tweezers (NOTs) can trap single proteins using local electromagnetic field enhancements at metal surfaces and therefore they are also subject to surface interactions. To probe these interactions, we consider the power dependence of the trapping stiffness at the limit of zero power, where an attractive or repulsive static force remains. We analyze various proteins with different charge and find that negatively charged proteins are attracted to the gold surface and positively charged proteins are repelled. We interpret this attraction as coming from local positive image charges on the gold adjacent to the negatively charged glass-water interface, as confirmed by finite-element Poisson equation simulations. This work shows a way to quantify the important impact of surface interactions in nanophotonic single molecule sensors of biomolecules and nanoparticles and to gauge their surface charge.

Keywords: single molecule, optical tweezers, label-free, surface interactions, electrostatic interactions

1. Introduction

Various methods have been used to localize nanoparticles, including proteins, for long-term single-particle studies without escape from diffusion, including electrokinetic traps [1], electrostatic traps [2], and nanoaperture optical

Original Content from this work may be used under the terms of the Creative Commons Attribution 4.0 licence. Any further distribution of this work must maintain attribution to the author(s) and the title of the work, journal citation and DOI.

tweezers (NOTs) [3]. By engineering the shape of the nanoaperture to have a strong local field intensity, NOTs have been shown to be capable of trapping dielectric objects in the single digit nanometer range (including single proteins) [4–22]. With this stable trapping, NOTs can be used to study unmodified individual proteins and their interactions without the need for labels or tethers for hours.

NOTs benefit by having significantly lower heating than their plasmonic particle antenna counterparts [23, 24]; however, they are still subject to surface interactions that have received only limited attention in past works. For example, polyethylene glycol surface layers were used to ensure that protein sticking was not contributing when the trapping of single proteins was demonstrated [5]. At the same time, it is interesting to note that the typical delay in the time to achieve

¹ Department of Electrical Engineering, University of Victoria, Victoria V8W 2Y2, British Columbia, Canada

² Center for Advanced Material & Related Technologies, University of Victoria, Victoria V8W 2Y2, British Columbia, Canada

³ Light-Matter Interactions for Quantum Technologies Unit, Okinawa Institute of Science and Technology Graduate University, Onna, Okinawa 904-0495, Japan

⁴ Advanced Optics and Photonics Laboratory, Department of Engineering, School of Science & Technology, Nottingham Trent University, Nottingham Trent NG11 8NS, England

⁵ These two authors contributed equally.

^{*} Author to whom any correspondence should be addressed.

trapping is of the order of minutes, so the particle takes a long time to enter the trap; in contrast, based entirely on diffusion and the concentration of nanoparticles, a trapping time many orders of magnitude shorter would be expected. This discrepancy suggests that surface electrostatic (ES) repulsion and/or thermophoresis are working against the optical trapping. Various strategies have been considered to overcome this limitation. For example, dielectrophoresis has been used in combination with NOTs to speed up the time to trap [25]. Electro-osmotic flow and thermally induced flow have also been used to assist in the manipulation of nanoparticles and biomolecules [11, 26].

Some part of the long time to trap may be attributed to thermophobic interactions with the higher local temperature at the trap [13, 27]. Another possible contribution to the interaction comes from ES effects at the surface [2]; however, quantification of this effect for NOTs has been lacking. Both optical tweezer and thermophoretic effects depend linearly on the intensity of the laser beam as this creates strong electromagnetic and thermal gradients; however, in the limit of zero laser intensity, only the ES response remains. Here, we analyze the dynamics of the NOT intensity fluctuations as a function of power and extrapolate to zero power to quantify the static interaction. We find that negatively charged proteins are attracted to the surface by ES effects and the opposite occurs for positively charged proteins, which we attribute to attractive image charges in the gold film that screen out the negative surface charge of the glass substrate in aqueous solution. This interpretation is supported by finite-element Poisson equation simulations.

2. Results

2.1. Spectral analysis

The usual theory accounting for the stochastic trajectory dynamics of optical tweezers considers a harmonic potential in the low Reynold's number (inertia free) limit for position *x*:

$$\gamma \dot{x} + kx = F(t), \tag{1}$$

where F(t) is the Langevin random thermal force term, γ is the Stokes' drag, and k is the spring constant. Harmonic analysis of this equation gives a Lorentzian power spectral density with corner frequency (i.e. the frequency at which the power spectral density is half of its low frequency value): [28]

$$f_{3-dB} = 1/\tau = k/(2\pi\gamma)$$
 (2)

where $f_{3-{\rm dB}}$ is the corner frequency of the power spectral density Lorentzian fit. The relation to τ , the autocorrelation exponential decay time constant, is given by the Wiener–Khinchin theorem.

A generalization of this approach to include thermophoretic and ES interactions gives:

$$k = k_{\rm s} + \frac{\mathrm{d}k_o}{\mathrm{d}I}I + \frac{k_{\rm t}}{\mathrm{d}I}I\tag{3}$$

where k_s , k_o and k_t are the surface ES, optical tweezers, and thermophoretic spring constants, and I is the optical intensity. The thermophoretic contribution is linearly proportional to the intensity because the temperature gradient scales linearly with the local heating from the laser [13]. If the Soret coefficient is negative, this is a thermophilic force; however, it is often reported that proteins are thermophobic at physiological temperatures [29]. The optical forces are also linearly proportional to the local intensity.

2.2. Analysis of past work on polystyrene(PS) nanoparticles

Past work considered the power dependence of trapping efficiency by looking at autocorrelation time and the data from that work are reproduced in figure 1(A) [30]. In that work, NOTs were used to trap 20 nm diameter PS particles. A linear extrapolation of $1/\tau$ to zero power shows a negative intercept. This means that the laser intensity has to be increased in order to achieve sufficient trapping force to overcome the surface ES force.

2.3. Analysis of proteins

We consider the trapping of three different proteins in PBS solution: Bovine serum albumin (BSA), Carbonic anhydrase (CA), Cytochrome C (CTC), ovalbumin, and trypsin. The schematic setup of trapping is shown in figure 1(B). Details are provided in the Methods section. Figures 2(A) and (B) shows the trapping events and corner frequencies for BSA. The dark blue curves use a moving with a window size of 0.1 s to reduce the high-frequency fluctuations. The trapping event is noted by increases in noise level and sometimes a stepalthough the step is dependent on exact alignment. The corner frequency can be found by two separate methods, first by fitting the power spectral density to a Lorentzian, by taking the autocorrelation and fitting the initial decay to extract a time constant using equation (2). We investigated whether plasma cleaning the sample prior to trapping, which makes the gold surface more hydrophilic, would impact the results. We found it did not change the intercept results.

The telegraphing observed in the BSA is typical for that protein as it undergoes conformational changes [5, 31, 32]. Considering that BSA has multiple states, we have taken the corner frequency combining all the data, but when we extract particular sections, we note the lower and higher states are nominally the same (to within 2.2%). The results of figure 2(C) were obtained from the three different authors by using two different optical trapping setups. We found the *y*-intercepts of the corner frequencies from 3 different experiments were around 10 Hz. In all cases, the analysis found a positive intercept for the corner frequency (and equivalently the inverse of the autocorrelation time constant) at zero laser power.

Figure 3 exhibits positive interceptions of CA, BSA, and ovalbumin with an isoelectric point smaller than 7. CA has an intercept of 13.80 Hz, BSA has an intercept of 7.25 Hz, and ovalbumin has an intercept of 2.51 Hz.

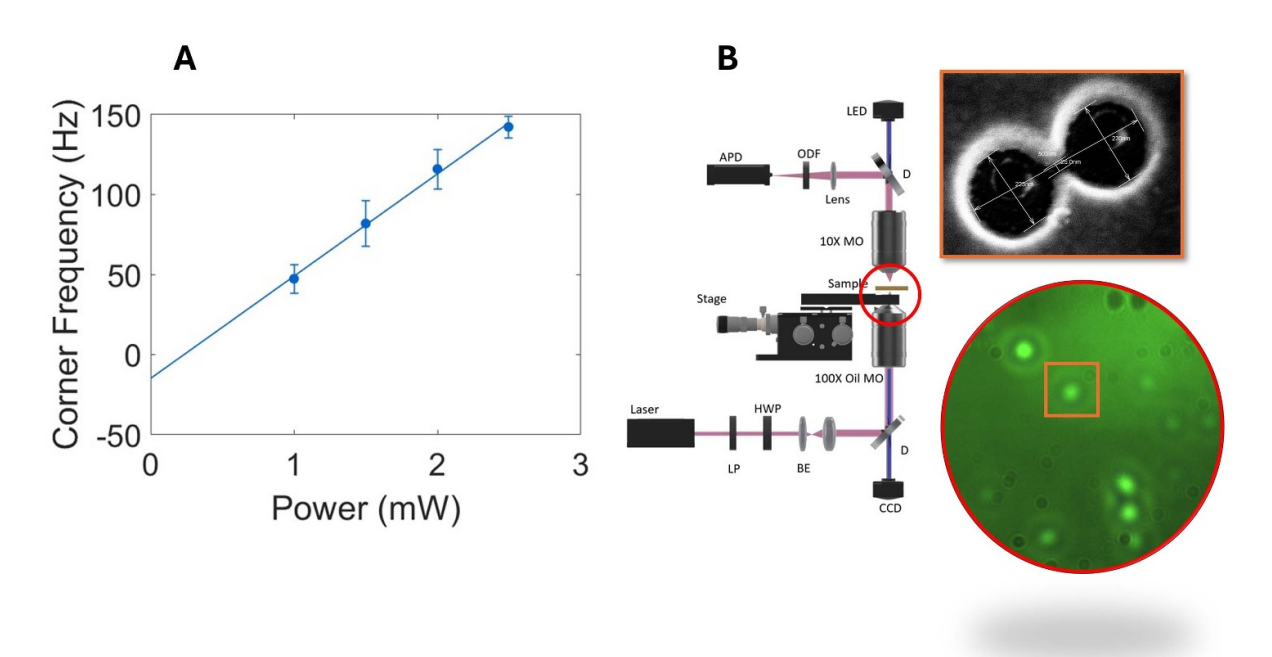


Figure 1. Extrapolated corner frequency at zero power for trapping of polystyrene nanoparticles. (A) Corner frequency extrapolated to zero power based on past work for trapping a 20 nm polystyrene sphere in a NOT. (B) Schematic of NOT setup. A scanning electron microscope (SEM) image of the double nanohole (DNH) structure (top right) and a CCD camera image of the sample region (bottom right) are shown for reference. LP = linear polarizer, HWP = half waveplate, BE = beam expander, CCD = charge coupled device, D = dichroic mirror, OI MO = oil immersion microscope objective, L = lens, ODF = optical density filter, APD = avalanche photodiode [30].

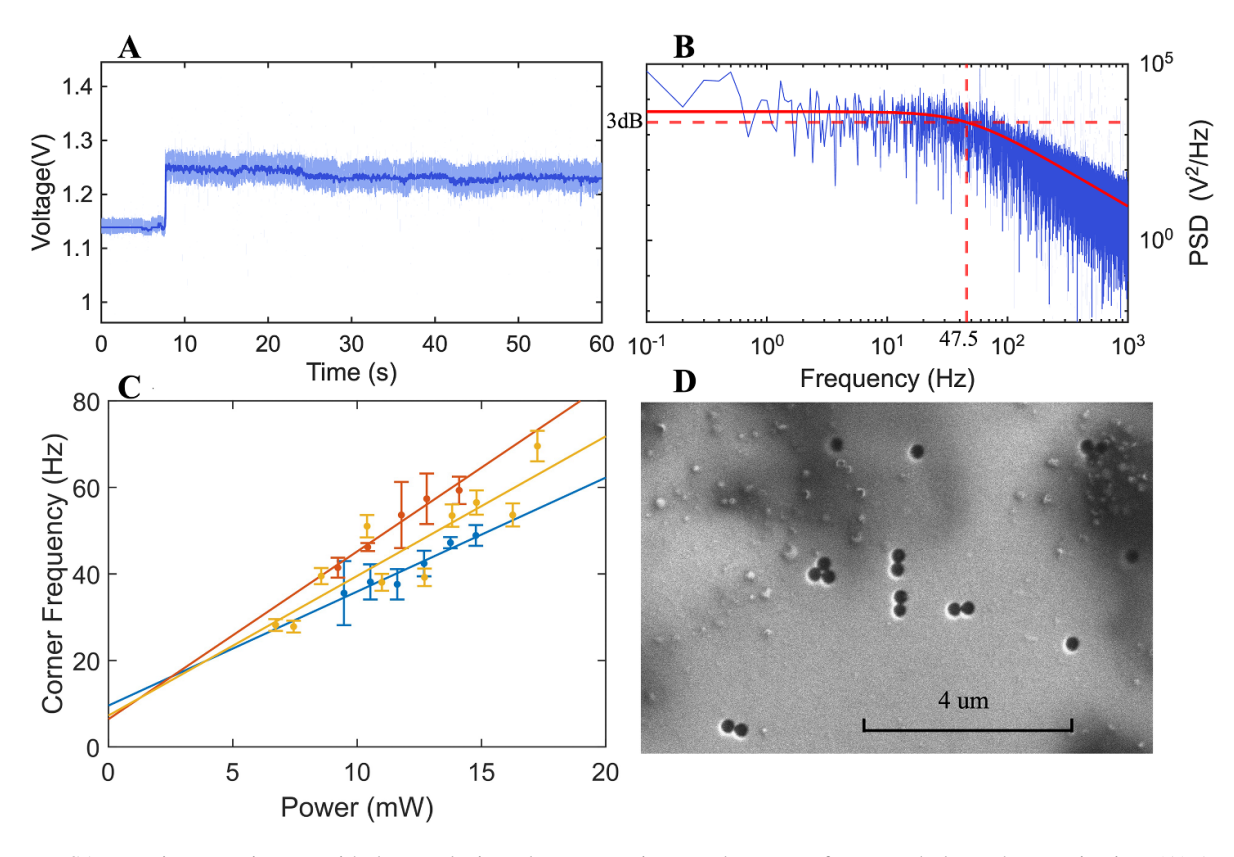


Figure 2. BSA Trapping experiments with data analysis and post-experiment substrate surface morphology characterization. (A) APD voltage measuring transmission through DNH with trapping of BSA; (B) power spectrum density and Lorentzian fitting curve, the dashed red lines show the 3 dB corner frequency at 47.5 Hz; (C) Corner frequency versus power of trapped BSA performed by three different authors using two optical tweezer setups with laser wavelengths of 850 nm (red) and 980 nm (yellow and blue), three solid lines are linear fits between power and corner frequency; (D) SEM image of a DNH gold substrate taken after usage for BSA trapping experiments.

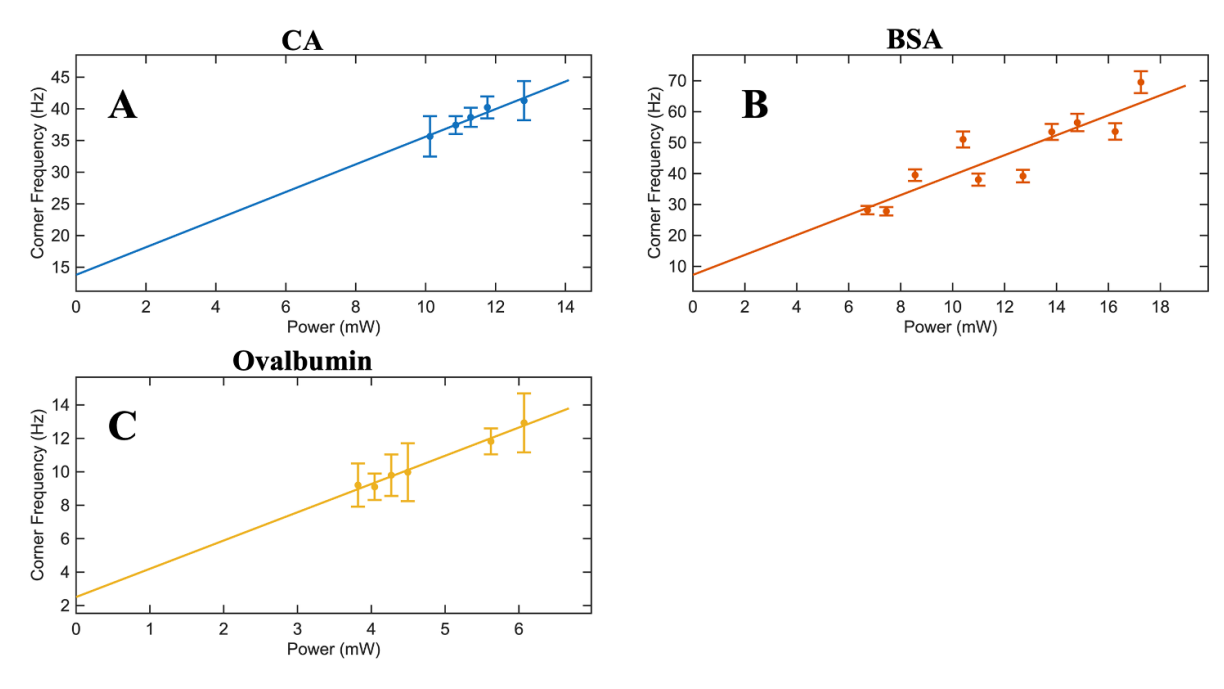


Figure 3. Extrapolated corner frequency to zero power with positive intercept for three different proteins. Corner frequency versus power plot of trapping (A) CA ($R^2 = 0.955$), (B) BSA ($R^2 = 0.911$), (C) ovalbumin ($R^2 = 0.984$).

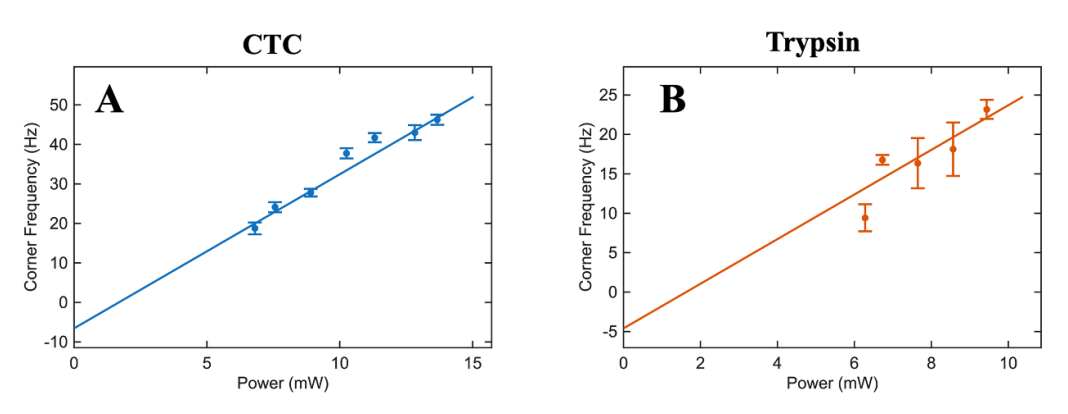


Figure 4. Extrapolated corner frequency to zero power with negative intercept for two different proteins. Corner frequency versus power plot of trapping (A) CTC ($R^2 = 0.953$), (B) trypsin ($R^2 = 0.794$).

Figure 4 shows negative interceptions of CTC and trypsin with an isoelectric point larger than 7. CTC has an intercept of $-6.56\,\mathrm{Hz}$, and trypsin has an intercept of $-4.60\,\mathrm{Hz}$. The corner frequency values cross through zero are around 2 mW, showing that this is the minimum power for the attractive optical trapping potential to overcome the electrostatic forces pulling the particle out of the trap. It should be noted that there is no physical meaning for negative corner frequency values.

A summary of the results for the five proteins analyzed is shown in table 1.

2.4. Numerical simulations

Details of the numerical simulation are found in the Methods section. In aqueous solution, the surface of silica glass adopts a large negative charge [33]. Gold has both negative [34] and positive [35] charge reported, but it has significantly less than glass, so we defined it as having no charge and a constant

Table 1. Properties of proteins used in the experiment.

Protein	Mass (kDa)	Isoelectric point	Charge (pH 7)	y-intercept
BSA	66	5.4	_	+
CA	29.2	5.5	_	+
Ovalbumin	45	4.5	_	+
CTC	14.3	9.6	+	_
Trypsin	23.3	10.5	+	_

potential. We observed that there is a screening in the gold of the field from the negative charge at the silica-water interface, which sets up a potential that will attract negatively charged particles towards the gold surface provided that they are small enough to avoid the repulsion by the glass-water interface. The special distribution of the simulated trapping potential is shown in figure 5.

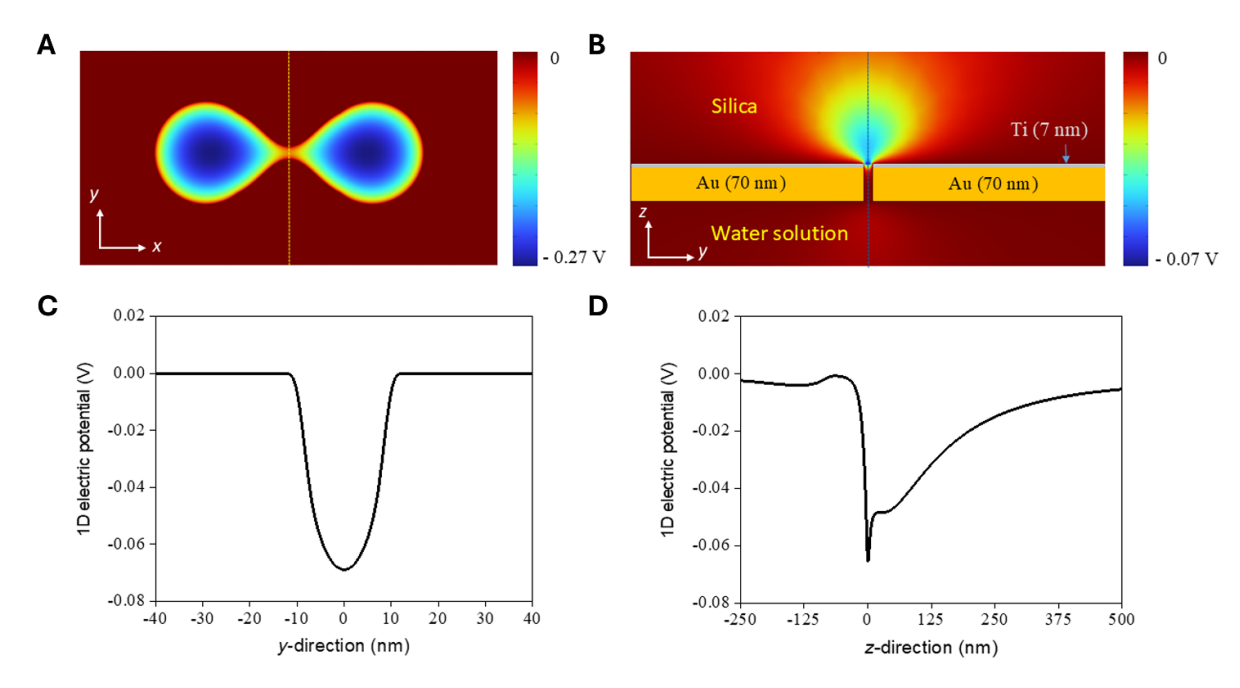


Figure 5. Finite element Poisson solutions showing the trapping potential towards the gold surface at the tips of a DNH for a negatively charged particle. The DNH structure in (A) and (B) is based on structure obtained by colloidal lithography (see Methods section) with 70 nm gold on 7 nm titanium on glass substrate immersed in an aqueous solution in a microwell. A scanning electron microscope image of the sample is shown in figure 1(B). 2D electric potential in the *y*-direction (C) and the *z*-direction (D).

3. Discussion

We note that the extrapolation to zero has also been used in past works that quantify the role of surfactant on thermophobic interactions in nanoaperture optical tweezers [13]. Here we have added an offset to account for interactions that are not dependent on the laser power (i.e. electrostatic interactions) [2]. We are unable to perform experiments at lower powers because the protein escapes from the trap due to thermal diffusion, as has been reported previously [36].

As shown here, early work on PS particles, which are negatively charged, had a negative intercept in the measurements, indicative of repulsive interactions. This was not discussed in that previous work [30]. The glass-water interface is negatively charged [33]. This induces positive image charges in the gold. However, the attractive region at the corner is too small for large particles like PS nanoparticles to enter, so they experience repulsion instead. Previous simulations have shown that the attractive optical trapping potential is concentrated near the corner of the nanostructure [37]. The voltage values, i.e. the ES potentials, are shown in figures 5(A)–(D) for different planes and 1D cuts. The potential a charged particle experiences is the product of the charge and voltage. Figure 5(C) shows that a negatively charged particle will be repelled from the central position between the cusps towards the gold surface at $-10 \,\mathrm{nm}$ or $+10 \,\mathrm{nm}$ along the y-direction. The potential energy will depend on the magnitude of the charge on the particle. For example, if the charge is that of a single electron, the difference in the potential at position y = 0 nm and y = 10nm is 0.07 eV, which is 3 times the thermal energy of 0.025 eV. Similarly, figure 5(D) shows that a negatively charged particle

at y = 0 nm will be pushed to positive z values (it cannot go to negative z values due to the pressence of the glass substrate). There is a flat part in the potential towards the top of the gold gap at 70 nm, the attractive potential for negatively charged particles toward the gold is weaker at this position. A positively charged particle will be attracted away from the gold surface where the optical field is highest by the negative charge of the glass-water interface, thereby pulling the particle out of the optical trap and requiring additional force to overcome the attraction towards the glass. Proteins, like BSA and CA, are attracted to the nanohole corner due to their small size and negative charge near neutral pH. As a result, a positive yintercept is obtained in the trapping data analysis, demonstrating a residual attractive potential even when the laser power is zero. In contrast, CTC, which is positively charged, is electrostatically repelled from the gold surface due to the positive image charges induced in the metal, resulting in a negative y-intercept in the analysis so that additional optical power is required to overcome the ES repulsion.

By analyzing the power dependence on the trapping stiffness and extrapolating it to zero power, we quantified the static interactions that govern the behavior of the protein near the gold surface. Negatively charged proteins are attracted to the gold surface, while positively charged proteins are repelled, which we attribute to local positive image charges on the gold. By establishing a method to measure these effects, this study provides insight into the fundamental forces governing nanoscale trapping, helping to improve the design of nanophotonic biosensors and enabling better control of optical trapping for the study of biomolecules and nanoparticles. It is possible to envision extending this experiment to a flow-cell setup

where the pH is varied to determine the isoelectric point of the trapped protein by determining for which pH the *y*-intercept crosses zero.

4. Conclusion

In this work, we have probed the interaction between surface charge and trapping of proteins in a NOT by extrapolating the trapping power spectral density corner frequency to its value at zero laser power. We observe that negatively charged proteins have a residual attraction and vice versa for a positively charged protein. We interpret this effect as coming from a positive screening in the gold due to the strong negative charge accumulation at the water-glass (substrate) interface. This work not only reveals the surface interactions relevant to nanophotonic trapping, but may also be used in the future to probe the charge properties of individual proteins with changes in environment.

5. Methods

5.1. Colloidal lithography of DNH

The glass slides $(76 \times 25.4 \times 1.0 \text{ mm}^3)$ were divided into thirds using a diamond scribe and cleaved. They were cleaned with 99% ethanol and dried with nitrogen gas. The slides were then sonicated in ethanol for 10 min, followed by rinsing with acetone, deionized water, and ethanol, with drying in between each step. A 1:100 mixture of 300 nm PS beads (Sigma-Aldrich, MFCD00131491 LB3) and ethanol was applied evenly to the slides, left to sit overnight for the ethanol to evaporate, leaving behind a mask of randomly arranged beads, including some dimers. The slides were plasma etched (Mantis QUBE system) for 170 s to control the cusp size. Next, a 7 nm titanium layer and a 70 nm gold layer were sputtered onto the slides. After 10 min of sonication in ethanol, the beads were removed using adhesive tape. The samples were rinsed with ethanol and dried with nitrogen gas, then cut into quarters using a diamond scribe and cleaned again.

5.2. Trapping solution

A 10 μ l portion of a 10 mg ml⁻¹ protein solution (BSA, Sigma-Aldrich, MWGF70-1KT; CA Sigma-Aldrich, C3943-100MG; CTC, Sigma-Aldrich, C7752-50MG; ovalbumin, Sigma-Aldrich, S7951-1MG; Strypsin, Sigma-Aldrich, A5503-1G) solution in 10 μ M PBS was added to a microwell formed by placing a 0.1 mm thick image spacer (Grace BioLabs, GBL-654008-100EA) onto a glass slide (Globe Scientific Inc., 1419-10). The microwell was then sealed with the DNH sample, with the gold surface facing downward.

5.3. Optical tweezers

For each experimental setup (two different laser wavelengths were used: 850 nm and 980 nm), the laser was collimated from

the fiber to a beam size of 2 mm and passed through a linear polarizer and a half-wave plate to allow for selection of any linear polarization state. The beam was then expanded to approximately 7 mm using a beam expander before being focused by an oil immersion microscope objective onto a DNH in the gold film inside of a microwell containing the nanoparticle solution. The polarization state was selected to maximize the transmission through the nanohole, as collected by a second microscope objective and focused onto an avalanche photodiode. An LED was used to illuminate the sample and allow for viewing the location of the nanoholes on the CCD camera. Dichroic mirrors were used to filter out the laser light from the LED and the camera paths. The laser power was measured with a photodetector prior to the microscope objective.

5.4. Software, statistical analysis, and data acquisition

All data analysis was performed using custom Python and MATLAB code. Data was collected at a sampling rate of kHz. The total number of trapping signals analyzed was 24. The root-mean-squared-deviation (RMSD) was calculated by dividing the same 5 s portion of the trapped signal into sections based on a window length of 5000. The RMSD was then divided by the mean of the trapped signal and an average of all the sections was taken. The coefficient of determination (R^2) was calculated to evaluate the goodness of the linear fit between corner frequency and trapping power.

5.5. Numerical simulations

commercial finite element modeling COMSOL Multiphysics version 6.2 was used for the ES potential simulations. A 3D model was established to solve the ES problems. The modeling process was governed by the fundamental Poisson's partial differential equations describing a connection between the electric field, E, the volume charge density, ρ , and the ES potential, V. Poisson's equation is given by $\nabla^2 V = -\rho/\varepsilon$ where ε is the relative permittivity, and the Efield serves as the gradient of the potential $V, E = -\nabla V$. The entire 3D ES domain was set at $2.0 \times 2.0 \times 2.0 \mu m^3$ cube, consisting of a single DNH at the center of the unit cell. Zero charge conditions were used on all outer ES domain's boundaries. The surface charge density of the silica-water interface within the DNH region was taken from experimental observations, and set as $\rho_s = -0.3 \text{ mC m}^{-2}$, approximately 2000 electrons μm^{-2} [33]. The thicknesses of gold and titanium metals were 70 nm and 7 nm, respectively. These full-metal domains are highly conductive; therefore, we set floating voltages over the entire metal's surfaces to be constant potential of 0 V. The relative permittivities of water and silica were taken from the material libraries of the ES module in COMSOL Multiphysics. The 3D model required 100 GB of memory to perform the calculation. The simulation solved Poisson's equation, which gave the potential felt by an infinitesimal charge.

Data availability statement

The data that support the findings of this study are openly available at the following URL/DOI: https://github.com/nanoplasmonics/surface.

Acknowledgments

The authors acknowledge the use of the facilities of the Centre for Advanced Materials and Related Technologies (CAMTEC). R G acknowledges funding from NSERC Discovery Grant RGPIN-2023-04-18 and JSPS Visiting Fellowship S23032. S N C and V G T acknowledge funding from OIST Graduate University. VGT acknowledges support by JSPS KAKENHI, Grant-in-Aid for Scientific Research (C), Project Number JP23K04618. C Y appreciates the support from the Academy of Medical Sciences (AMS) Springboard Award (SBF0010\1008). RG thanks Matthew Peters for discussions on this topic. S N C and V G T thank the OIST Scientific Computing and Data Analysis section.

Conflict of interest

The authors declare no competing interests.

Author contributions

Sherin George

Investigation (lead), Formal analysis (lead), Writing – original draft (lead)

Tianyu Zhao

Investigation (lead), Formal analysis (lead), Data curation (lead), Writing – original draft (lead)

Keiran Letwin Investigation (lead)

Viet Giang Truong © 0000-0003-3589-7850 Investigation (supporting), Formal analysis (lead), Software (lead), Writing – original draft (supporting)

Naser Helmi

Formal analysis (supporting), Methodology (supporting)

Síle Nic Chormaic © 0000-0003-4276-2014 Investigation (supporting), Formal analysis (lead), Software (lead), Writing – original draft (supporting)

Cuifeng Ying © 0000-0002-7279-1388 Formal analysis (supporting), Writing – original draft (supporting)

Reuven Gordon © 0000-0002-1485-6067 Conceptualization (lead), Formal analysis (supporting), Writing – original draft (lead)

References

- [1] Cohen A E and Moerner W 2006 Suppressing Brownian motion of individual biomolecules in solution *Proc. Natl* Acad. Sci. 103 4362–5
- [2] Krishnan M, Mojarad N, Kukura P and Sandoghdar V 2010 Geometry-induced electrostatic trapping of nanometric objects in a fluid *Nature* 467 692–5
- [3] Juan M L, Gordon R, Pang Y, Eftekhari F and Quidant R 2009 Self-induced back-action optical trapping of dielectric nanoparticles *Nat. Phys.* 5 915–9
- [4] Pang Y and Gordon R 2011 Optical trapping of 12 nm dielectric spheres using double-nanoholes in a gold film Nano Lett. 11 3763–7
- [5] Pang Y and Gordon R 2012 Optical trapping of a single protein *Nano Lett.* **12** 402–6
- [6] Berthelot J et al 2014 Three-dimensional manipulation with scanning near-field optical nanotweezers Nat. Nanotechnol. 9 295–9
- [7] Kerman S, Chen C, Li Y, Van Roy W, Lagae L and Van Dorpe P 2015 Raman fingerprinting of single dielectric nanoparticles in plasmonic nanopores *Nanoscale* 7 18612–8
- [8] Jensen R A, Huang I-C, Chen O, Choy J T, Bischof T S, Lončar M and Bawendi M G 2016 Optical trapping and two-photon excitation of colloidal quantum dots using bowtie apertures ACS Photonics 3 423-7
- [9] Raza M U, Peri S S S, Ma L-C, Iqbal S M and Alexandrakis G 2018 Self-induced back action actuated nanopore electrophoresis (SANE) *Nanotechnology* 29 435501
- [10] Yoo D et al 2018 Low-power optical trapping of nanoparticles and proteins with resonant coaxial nanoaperture using 10 nm gap Nano Lett. 18 3637–42
- [11] Kotnala A, Kollipara P S, Li J and Zheng Y 2019 Overcoming diffusion-limited trapping in nanoaperture tweezers using opto-thermal-induced flow *Nano Lett.* 20 768–79
- [12] Yoon S J, Song D I, Lee J, Kim M-K, Lee Y-H and Kim C-K 2020 Hopping of single nanoparticles trapped in a plasmonic double-well potential *Nanophotonics* 9 4729–35
- [13] Jiang Q, Rogez B, Claude J-B, Baffou G and Wenger J 2020 Quantifying the role of the surfactant and the thermophoretic force in plasmonic nano-optical trapping Nano Lett. 20 8811–7
- [14] Kotsifaki D G, Truong V G and Nic Chormaic S 2020 Fano-resonant, asymmetric, metamaterial-assisted tweezers for single nanoparticle trapping *Nano Lett.* 20 3388–95
- [15] Li N, Cadusch J, Liu A, Barlow A J, Roberts A and Crozier K B 2021 Algorithm-designed plasmonic nanotweezers: quantitative comparison by theory, cathodoluminescence and nanoparticle trapping Adv. Opt. Mat. 9 2100758
- [16] Yang W, van Dijk M, Primavera C and Dekker C 2021 Fib-milled plasmonic nanoapertures allow for long trapping times of individual proteins iScience 24 103237
- [17] Ying C et al 2021 Watching single unmodified enzymes at work (arXiv:2107.06407)
- [18] Peri S S S *et al* 2019 Detection of specific antibody-ligand interactions with a self-induced back-action actuated nanopore electrophoresis sensor *Nanotechnology* **31** 085502
- [19] Peri S S S, Sabnani M K, Raza M U, Urquhart E L, Ghaffari S, Lee J S, Kim M J, Weidanz J and Alexandrakis G 2020 Quantification of low affinity binding interactions between natural killer cell inhibitory receptors and targeting ligands with a self-induced back-action actuated nanopore electrophoresis (SANE) sensor *Nanotechnology* 32 045501
- [20] Wu B, Lou Y, Wu D, Min Q, Wan X, Zhang H, Yu Y, Ma J, Si G and Pang Y 2022 Directivity-enhanced detection of a single nanoparticle using a plasmonic slot antenna *Nano Lett.* 22 2374–80

- [21] Hong C and Ndukaife J C 2023 Scalable trapping of single nanosized extracellular vesicles using plasmonics *Nat. Commun.* 14 4801
- [22] Yousefi A et al 2023 Optical monitoring of in situ iron loading into single, native ferritin proteins Nano Lett. 23 3251–8
- [23] Verschueren D V et al 2018 Label-free optical detection of dna translocations through plasmonic nanopores ACS Nano 13 61–70
- [24] Jiang Q et al 2020 Adhesion layer influence on controlling the local temperature in plasmonic gold nanoholes Nanoscale 12 2524–31
- [25] Babaei E, Wright D and Gordon R 2023 Fringe dielectrophoresis nanoaperture optical trapping with order of magnitude speed-up for unmodified proteins *Nano Lett.* 23 2877–82
- [26] Hong C, Yang S and Ndukaife J C 2020 Stand-off trapping and manipulation of sub-10 nm objects and biomolecules using opto-thermo-electrohydrodynamic tweezers *Nat. Nanotechnol.* 15 908–13
- [27] Jiang Q, Rogez B, Claude J-B, Baffou G and Wenger J 2019 Temperature measurement in plasmonic nanoapertures used for optical trapping ACS Photonics 6 1763–73
- [28] Svoboda K and Block S M 1994 Biological applications of optical forces Annu. Rev. Biophys. Biomol. Struct. 23 247–85
- [29] Iacopini S and Piazza R 2003 Thermophoresis in protein solutions Europhys. Lett. 63 247

- [30] Kotnala A and Gordon R 2014 Quantification of high-efficiency trapping of nanoparticles in a double nanohole optical tweezer *Nano Lett*. 14 853–6
- [31] Peters M *et al* 2024 Energy landscape of conformational changes for a single unmodified protein *npj Biosensing* 1 14
- [32] Letwin K, Peters M and Gordon R 2025 Conformational stability at low temperatures using single protein nanoaperture optical tweezers *J. Phys. Chem. B* 129 2402–7
- [33] Behrens S H and Grier D G 2001 The charge of glass and silica surfaces *J. Chem. Phys.* **115** 6716–21
- [34] Chai L and Klein J 2009 Interactions between molecularly smooth gold and mica surfaces across aqueous solutions *Langmuir* **25** 11533–40
- [35] Tivony R and Klein J 2016 Probing the surface properties of gold at low electrolyte concentration *Langmuir* 32 7346–55
- [36] Zehtabi-Oskuie A, Bergeron J G and Gordon R 2012 Flow-dependent double-nanohole optical trapping of 20 nm polystyrene nanospheres Sci. Rep. 2 966
- [37] Ghorbanzadeh M, Jones S, Moravvej-Farshi M K and Gordon R 2017 Improvement of sensing and trapping efficiency of double nanohole apertures via enhancing the wedge plasmon polariton modes with tapered cusps ACS Photonics 4 1108–13